J Solid State Electrochem (2014) 18:3099–3109
DOI 10.1007/s10008-013-2375-x

ORIGINAL PAPER

TiO_2 and Al_2O_3 nanoporous oxide layers decorated with silver nanoparticles—active substrates for SERS measurements

Marcin Pisarek · Marcin Holdynski · Agata Roguska · Andrzej Kudelski · Maria Janik-Czachor

Received: 8 November 2013 / Revised: 17 December 2013 / Accepted: 27 December 2013 / Published online: 1 February 2014

Abstract Self-organized nanoporous oxide layers (TiO_2, Al_2O_3) exhibiting specific properties, obtained by anodic oxidation at a constant voltage in neutral electrolyte, may serve as attractive SERS substrates for investigating the interactions between an adsorbate and adsorbent, or as a stable platform for detecting various organic compounds. This paper presents the influence of the size of the nanotubes/nanopores and the structure of the porous oxide layers on the SERS enhancement factor, E_F. We used pyridine and mercaptobenzoic acid as probe molecules, since they have a large cross-section for Raman scattering. To characterize the morphology and structure of the oxide layer substrates, before and after vacuum vapor deposition of silver nanoparticles, we applied scanning electron microscopy, X-ray diffraction and surface analytical techniques: AES, XPS and SERS. The results obtained show that for the same amount of Ag (0.02 mg/cm^2) the size of the nanopores significantly affects the E_F, which reaches, at a properly chosen nanopore size, distinctly higher values than that characteristic of a standard silver surface roughened by electrochemical cycling, i.e. $E_F > 10^6$. The new Ag/MeO_x–NT composites layer, ensure a good reproducibility of the SERS measurements and exhibit stability over a limited period of time.

Keywords SERS active substrates · TiO_2 and Al_2O_3 nanotubes: MeO_x-NT · Pyridine · Mercaptobenzoic acid

M. Pisarek (✉) · M. Holdynski · A. Roguska · M. Janik-Czachor
Institute of Physical Chemistry, Polish Academy of Sciences, Kasprzaka 44/52, 01-224 Warsaw, Poland
e-mail: mpisarek@ichf.edu.pl

A. Kudelski
Faculty of Chemistry, University of Warsaw, Pasteur 1, 02-093 Warsaw, Poland

Introduction

The growing interest in titania and alumina nanoporous materials is due to their wide application in such fields as photocatalysis (TiO_2) [1–3], electrocatalysis (TiO_2) [4–6], lithography (Al_2O_3) [7, 8] and optoelectronics (TiO_2, Al_2O_3) [3, 6, 9], and also as self-cleaning coatings (TiO_2) [3], bio-sensor coatings (TiO_2) [10] and biomedical materials (TiO_2) [11–13]. Nanoporous layers of alumina are widely used as 'templates/matrices' for creating metallic nanofibres, semi-conductors and conductive polymers [7, 8]. The use of anodic oxidation (notably, anodic polarization at a constant potential) as a method of forming nanostructured oxide layers on metals affords numerous possibilities for controlling their morphology. The anodic oxidation of Ti and Al in neutral electrolytes (pH=7.4) containing fluorides is a typical electrochemical method of surface modification allowing oxide layers of varying thickness, homogeneous chemical composition and subtle nano-porosity to be obtained [3, 8, 13, 14]. The addition of a suitable concentration of fluorides to the electrolyte ensures a porous morphology in the form of nanotubes of titanium and aluminium oxides (a 'honeycomb' structure) [3, 8, 13, 15]. This method makes it possible to form TiO_2 and Al_2O_3 nanotubes having a diameter from a few dozen to several hundred nanometers and a height of a few micrometers, with the nanotubes/nanopores oriented perpendicular to the substrate [3, 7, 8, 13–18]. Such a wide range of diameters makes it possible to control the porosity and surface properties of a given material. The possibility of introducing new chemical and physical properties to titanium and aluminium oxides by creating orderly nanoporous structures using the anodic polarization method, as well as that of covering the porous substrates with SERS-active metals such as Ag, Cu or Au, may lead specifically to the fabrication of attractive SERS substrates [17–23].

The SERS method (surface-enhanced Raman spectroscopy) makes it possible to obtain information on metal–gas systems or metal–electrolyte systems. The huge enhancement coefficients of the spectrum intensity for molecules adsorbed onto the surface make it possible in some cases to obtain spectra for molecules from an aqueous solution having a concentration of less than 10^{-7} M. That enhancement is dependent on the effective Raman scattering cross-section, the wavelength of the incident radiation, the nature of the metallic surface and the physicochemical properties of the molecule under investigation. In the SERS technique, the orientation of the molecule with respect to the surface of the metal, and the distance between its functional groups from the surface on which it was adsorbed, play a key role in exciting particular Raman bands. This circumstance makes it possible to obtain specific information on the structure of a compound adsorbed onto the surface of a solution/solid and on its orientation in relation to the substrate. Research on SERS spectra is usually conducted on an electrochemically roughened metal surface. Numerous practical applications of the SERS method have led, however, to a search for new surfaces which provide a higher SERS spectrum enhancement coefficient, or better surface reproducibility [24–26]. Theoretical reflections aimed at explaining the very large enhancement of the SERS signal have not been completely satisfactory to date. The models proposed must, after all, explain a whole series of effect such as: the strong dependence of enhancement on the roughness of the metal surface, the decay of the signal together with the distance of the compound under study (adsorbate) from the surface, the strong depolarization of SERS bands and the dependence of the SERS enhancement coefficient on the frequency of the incident wave. Other effects which should also be explained by a well-defined model of the SERS phenomenon include the dependence of SERS intensity on the angle of incidence of the exciter radiation, and the large change in the spectrum observed with a change in the arrangement of the adsorbed molecules. It is currently accepted that the main cause of enhancement is the coincidence of two effects: an electromagnetic effect and a chemical effect, where the electromagnetic effect is dominant [27].

The theory explaining the electromagnetic effect draws on a dynamic model of the induction dipole: the laser radiation falling on the surface of the metal excites the oscillations of what are known as surface plasmons (collective oscillations of electrons in the surface layer of the metal). In order to obtain surface enhancement, there must be a suitable roughening at the surface of the metal. The intensity of Raman scattering increases with the voltage of the electromagnetic field in the vicinity of the very small metallic clusters, and especially, in the fissures between them. Surface plasmons occur in irregularities on the metal surface, which dimensions range from a few to several hundred nanometers. The enhancement effect occurs when an incident photon resonates with the oscillation of the conduction electrons near the surface. At that time, a very strong electric field is induced, which causes the increase in the intensity of the spectrum. Surface enhancement is, therefore, possible in an arrangement which involve an adsorbed molecule and a roughened surface substrate [28, 29].

The second theory explaining the SERS phenomenon takes into account chemical factors, including the charge transfer effect. This involves the fact that electrons can be transferred from the highest filled level in an adsorbed molecule to the Fermi level of a metal, or from the Fermi level of a metal to the lowest unfilled level in the molecule. One argument in favour of this mechanism is that a dependence has been observed between the intensity of the Raman bands recorded in SERS spectra and the external electrical potential applied [18, 19].

The aim of this work is to test whether:

1. SERS investigations with a probe molecule (pyridine, mercaptobenzoic acid - MBA) adsorbed on the Ag/MeO_x–NT composite layers provide spectroscopic data for determining the influence of the size of the nanotubes on the SERS enhancement factor (E_F);
2. the crystalline structure of the nanoporous oxide layer influence the interaction between adsorbate and adsorbent, and thus affects the SERS spectra as well;
3. the Ag/MeO_x–NT composite layers are stable substrates over a definite period of time and hence provide reproducible SERS results.

Experimental

Titanium and aluminium nanoporous oxide layers were fabricated by the electrochemical anodization of Ti or Al samples (Ti and Al foil 0.25 mm thick, 99.5 % purity) in an optimized mixture of an electrolyte: NH_4F (0.86 wt.%)+DI water (47.14 wt.%)+glycerol (52 wt.%) for Ti and 1 M $(NH_4)_2SO_4$+0.2 wt.% NH_4F for Al. After anodization, the samples were rinsed with DI water, few hours—TiO_2 or rinsed 15 min in an ultrasonic bath—Al_2O_3 finally dried in air. Subsequently, thermal annealing was performed at 450 and 650 °C for 3 h to transform the TiO_2 nanotubes structure from amorphous (after anodic oxidation) to crystalline (anatase, rutile).

Both the alumina and titania nanotubes were partly covered with an Ag deposit by the sputter deposition technique in a vacuum at a pressure of 3×10^{-3} Pa (the evaporation method), using a JEE-4X JEOL device, in a configuration perpendicular to the surface of the samples. The average amount of metal deposited per square centimeter (0.02 mg/cm^2) was estimated as the mass gain of the samples during the metal deposition process divided by the geometric surface area. Certainly, both the true average and local amount of the metal deposits may actually vary substantially due to the highly developed

specific surface area of the oxide substrates and the resulting non-uniform distribution of the metal deposits.

For the morphological characterization of the samples after their anodization, annealing and Ag deposition, examinations were carried out with a scanning electron microscope (a FEI NovaNanoSEM 450 and a Hitachi S-5500).

X-ray powder diffraction data were collected on a Philips X'Pert Pro diffractometer fitted with a X'Celerator detector using Ni-filtered Cu Kα radiation (λ_1=1.54056 Å and λ_2= 1.54439 Å). Data were collected on a flat plate θ/θ geometry on a Pt-coated sample holder. Calibration was carried out with an external Si standard. All data presented here were collected in the 2θ range 5–115°, in intervals of 0.0167°, with a scan time of 200 s per interval.

The chemical composition of the oxide layers before and after silver deposition process was examined using Auger electron microanalysis and photoelectron spectroscopy, with a Microlab 350 (Thermo Electron) having a lateral resolution of about 20 nm for AES and several millimeters for XPS. The chemical state of surface species was identified using the high-energy resolution spherical sector analyser of the Auger and XPS spectrometer (the maximum energy resolution is 0.83 eV for the XPS method). The appropriate standards for AES and XPS reference spectra were also used. XPS spectra were excited using AlK_α ($h\nu$=1486.6 eV) radiation as a source. The high-resolution spectra were recorded using 40 eV pass energy. A linear or Shirley background subtraction was made to obtain the XPS signal intensity. The peaks were fitted using an asymmetric Gaussian/Lorentzian mixed function. The measured binding energies were corrected in reference to the energy of C 1 s at 285 eV. Avantage-based data system software (Version 4.16) was used for data processing.

Raman spectra were collected with a Horiba Jobin–Yvon Labram HR800 spectrometer equipped with an Olympus BX40 microscope with a ×50 long distance objective, 600 grooves/mm holographic grating and a Peltier-cooled (1024×256 pixel) CCD detector. A He-Ne laser (632.8 nm) provided the excitation radiation.

Reference SERS-active metal samples Ag ref. were prepared by electrochemical roughening of a pure Ag sheet. The roughening of the Ag was carried out in a conventional three-electrode cell with a large platinum sheet as the counter-electrode and an Ag/AgCl (0.1 M KCl) electrode as a reference (all potentials are quoted versus this electrode); more details are given in [30].

Results and discussion

Characterization of the self-organized porous oxide substrates

The optimal anodization conditions applied resulted in the formation of TiO_2 and Al_2O_3 nanotubes ("hollow cylinders") arranged perpendicular to the substrate. The shape and diameter of the nanopores strictly depend on the type of electrolyte and the concentration of the fluoride ions, what has been described in detail elsewhere [3, 13, 15], and on the final anodic voltage applied, V_{max}.

Figure1 shows the effect of anodic voltage V_{max} on the average diameter of the nanopores. As can be seen for TiO_2, the V_{max} strongly affects the size of nanotubes, which increases with voltage, from about 20 nm at 5 V to almost 120 nm at 30 V. The dependence is approximately linear; the value of the correlation coefficient R^2 is 0.99. For alumina it was not possible to produce substrates with such a wide range of pore diameters because the used electrolyte worked only in a narrow range of final voltage V_{max}. Preparation of larger nanopores for Al_2O_3 is possible if a different type of electrolyte based on acidic solutions will be applied [8, 31]. However, the used electrolyte makes it possible to form nanoporous structures of alumina with similar pore diameters as those for titania, as can be seen in Fig. 1. This provides a chance to compare some of the SERS results for both oxides at roughly the same nanotube diameter.

Scanning electron microscopy (SEM) examinations revealed that the nanotubes were open at the top (see Fig. 2, top view), and closed from the bottom (see Fig. 3b, insert). The TiO_2 nanotubes are separated from each other, in contrast to the Al_2O_3 porous structure (Fig. 2c) [13, 18, 19]. The height of the oxide layer after anodization process is about 1 μm for TiO_2 nanotubes [13] and ~1.5 μm for Al_2O_3 nanoporous structure [18].

Usually as-prepared nanoporous oxides obtained by anodic oxidation were found to have amorphous structure [3]. The TiO_2 nanotubes were annealed in air at 450 °C, or 650 °C, to transfer the amorphous structures to crystalline phases. This may significantly influence the properties of the oxide layers

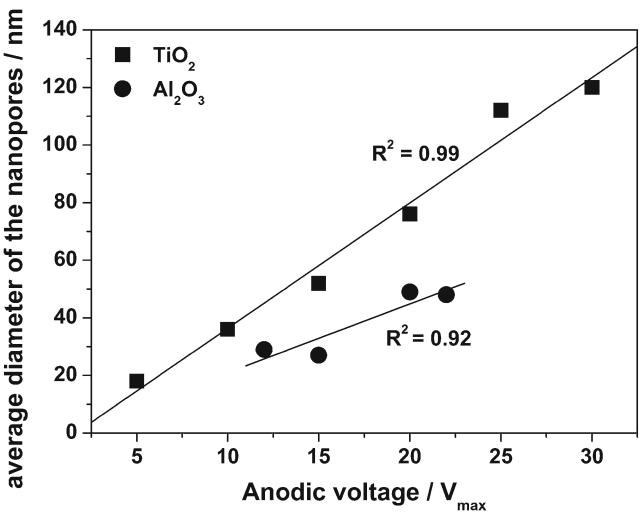

Fig. 1 Effect of anodic voltage V_{max} on average diameter of nanopores (nanotubes)

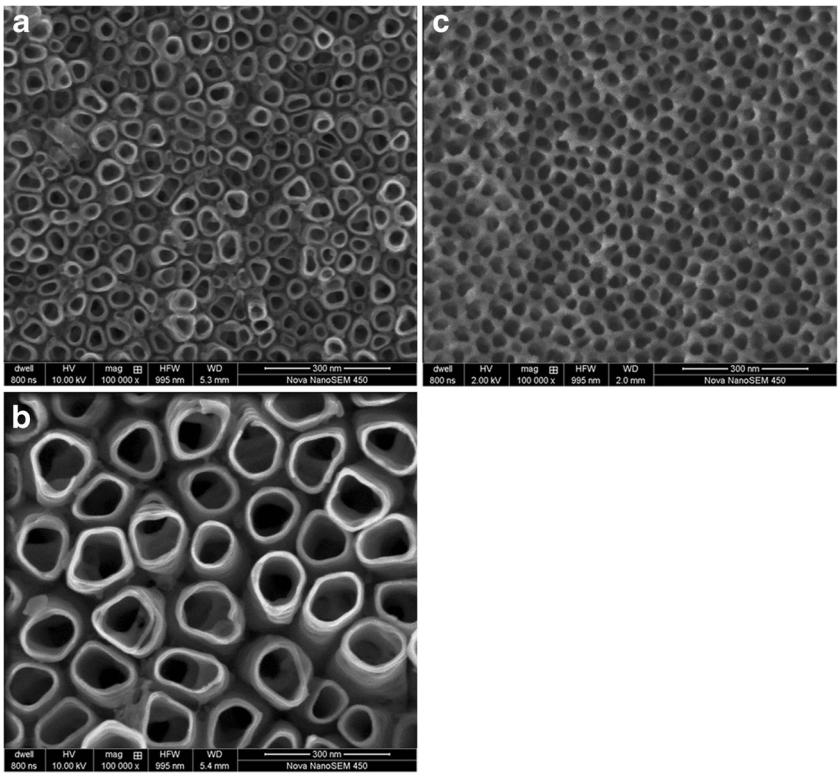

Fig. 2 Typical examples of the nanoporous structures of titania (**a** 10 V, **b** 25 V) and alumina (**c** 15 V) after the anodization process

(stability, electrical properties) thus making them suitable, for example, as active platforms for SERS measurements.

The X-ray diffraction (XRD) patterns for the as-anodized samples revealed characteristic reflections from the Ti and Al metals (substrates), Fig. 3. No evidence of extra peaks in the patterns suggests that the as-anodized oxides may be amorphous, which is in close agreement with the data from the literature [13, 18, 32, 33]. Since the thickness of the nanoporous oxide layers is only ~1–2 μm [13, 18], the characteristic bump of the amorphous phase typically seen at low angles is not visible here.

Annealing of TiO_2 NT/Ti samples in air at 450 or 650 °C transforms their amorphous structure into a crystalline one: to anatase at the lower temperature and the mixture of anatase and rutile at the higher temperature. See the results in Fig. 3a, where we can clearly distinguish the signals for those two phases. This is in agreement with existing literature data which suggest that the phase transition from anatase to rutile takes place at an annealing temperature of about 550–600 °C [13, 18, 33, 34]. The thermal treatments applied lead to a change of the titania crystal structure (which may in turn influence the electronic structure of the Ag nanoparticles deposited on such substrate, see discussion below). In contrast to the titania, the applied temperatures of annealing were too high for porous alumina layer, because the melting point of pure aluminium is about 660 °C, thus in further studies, we have focused on the use of alumina in amorphous form, see Fig. 3b. A detailed discussion on this subject is given further on.

In order to get a more insight into the chemical state of titanium and aluminium in the metals–oxygen surface compounds, XPS measurements for nonporous layers were performed. The results confirm that TiO_2 and Al_2O_3 are the main component of the annealed Ti and anodized Al surfaces, respectively. Deconvolution of the main XPS signals for metals: Ti 2p, Al 2p suggested that some lower oxides are also present, see Table 1.

Morphology of the Ag/MeO_x–NT composite layers

Figure 4 shows typical SEM images of TiO_2 (V_{max}=10 V (a) and 25 V (b)) and Al_2O_3 (V_{max}=15 V (c)) nanoporous layers covered with 0.02 mg/cm^2 of Ag. Careful inspection of Fig. 4a reveals that the sputter-deposited silver forms a thin solid coating on the top of the TiO_2 nanotubes (10 V) which is composed of Ag nanoparticles. The diameter of these particles is below 100 nm. The Ag deposit seems to completely cover the nanoporous oxide layer. In the case of the TiO_2 substrate with a larger diameter of pores, e.g. more than 100 nm, the Ag particles are located mainly on the top of the nanotubes. Figure 4b shows the distribution of Ag nanoparticles on the top of the TiO_2 nanotubes—V_{max}=25 V (light contrast—BSE image). The Al_2O_3 nanoporous layer covered with 0.02 mg/cm^2 Ag exhibits quite a different morphology (see Fig. 4c, SE image). Single Ag particles form a network over the nanopores which consists of small Ag nanoparticles, below 50 nm in diameter. A careful analysis of the above SEM data

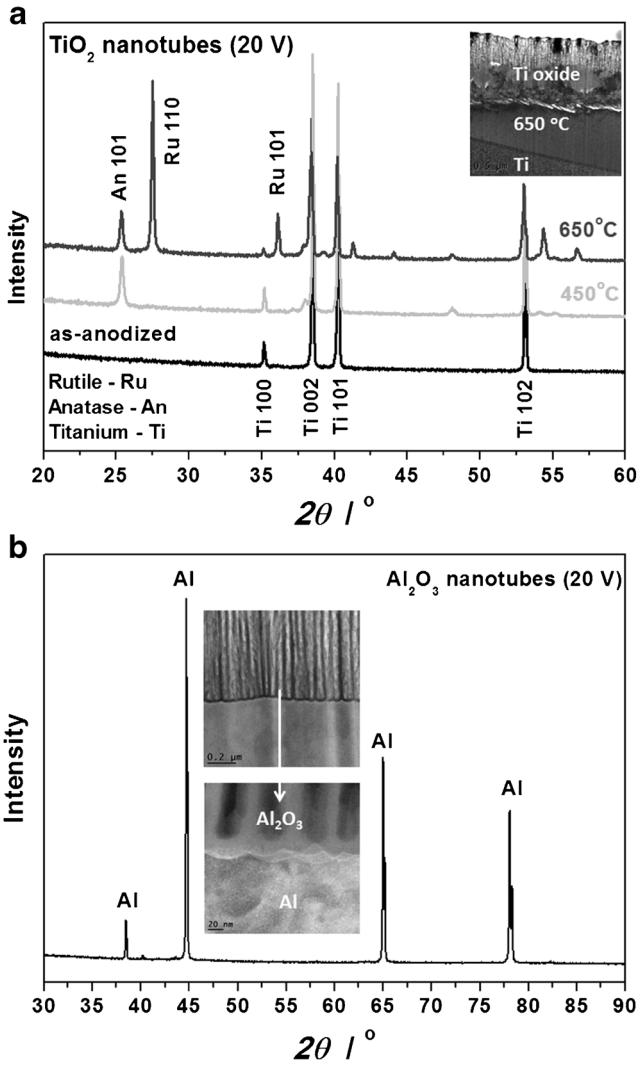

Fig. 3 Typical XRD patterns for TiO_2/Ti sample before (as-anodized) and after heat treatment (**a**) and for Al_2O_3/Al sample in as-anodized state (**b**). The *inserts* show cross-sectional views of the oxide layers

suggests that the diameters of the nanopores have been modified by the Ag particles, which are distributed non-homogenously over the nanoporous oxide surfaces. Figure 4d shows the surface morphology of a pure Ag reference sample. That sample was obtained using a common roughening procedure (oxidation–reduction cycling ORC, see the Experimental section). All the morphologies obtained are characterized by a large specific surface area, which is one of the most important factors affecting the intensity of the SERS spectra [35, 36]. Such arrays of Ag particles—coupled electromagnetically to each other—may produce strong resonances; therefore, our substrates may be superior for SERS applications [19–22, 28, 37].

Table 1 XPS results for titania and alumina NTs layers

	O 1 s/eV	Chemical state	Total atomic concentration/%
Ti $2p_{3/2}$/eV			
459.0 (major compound)	530.3	Ti^{4+} (TiO_2)	Ti—31.9
460.0 (minor compound)		TiO_x	O—68.2
Al 2p/eV			
74.5 (major compound)	531.7	Al^{3+} (Al_2O_3)	Al—40.0
76.0 (minor compound)		AlO_x	O—60.0

Chemical composition of the Ag/MeO_x–NT composite layers (AES, XPS)

Figure 5a shows Auger spectrum measured within a kinetic energy window of 200–550 eV on the Ag/TiO_2 NT/Ti sample prepared at V_{max}=20 V and covered with 0.02 mg Ag/cm^2. The Auger MNN reference signal of Ag corresponds to the position of the Ag signals measured locally on the Ag particles on the sample surface. Moreover, one can also see signals from oxygen (KLL) and titanium (LMM), suggesting that the titania substrate was also excited during the Auger electron emission process. This infers that the Ag deposit did not completely cover the surface of the sample (compare Fig. 4b). The high-resolution titania reference spectrum, which is also given, suggests that the titanium in the composite layer is bound to oxygen.

The high-resolution XPS spectrum for the Ag/Al_2O_3-NT/Al sample, confined to the Ag window (Fig. 5b), gives position of the binding energies of Ag 3d doublet peaks at 368.6 eV (Ag $3d_{5/2}$) and 374.6 eV (Ag $3d_{3/2}$). According to the literature [38], the Ag $3d_{5/2}$ binding energy for Ag is approximately 368.3 eV. This implies that the Ag particles located on the surface of the Ag/Al_2O_3 NT layer are metallic silver. A small shift of the main Ag peak of Ag $3d_{5/2}$ (about 0.5 eV) and its broadening as compared to that for the reference Ag suggest that the XPS signals of Ag are probably modified by the interaction of the Ag nanoparticles with the Al_2O_3 substrate. This may be induce by the shift of the Fermi level in the deposited silver particles which was indirectly confirmed by local AES measurements and SERS investigations in the course of our previous studies [17, 19].

SERS measurements

The titania and alumina nanotubes/nanopores without any Ag deposit are totally SERS inactive. Therefore, we confine our discussion below to the Ag/MeO_x–NT composite layers only.

In order to test the effect of the titanium oxide structure substrate, rutile vs. anatase, on the electronic properties of the silver nanoparticles deposited on these substrates, SERS measurements were performed for the samples with similar amount of silver deposit (0.01 and 0.015 mg/cm^2). There were no significant changes in the position and shape of the characteristic doublet of adsorbed pyridine on the titanium-based

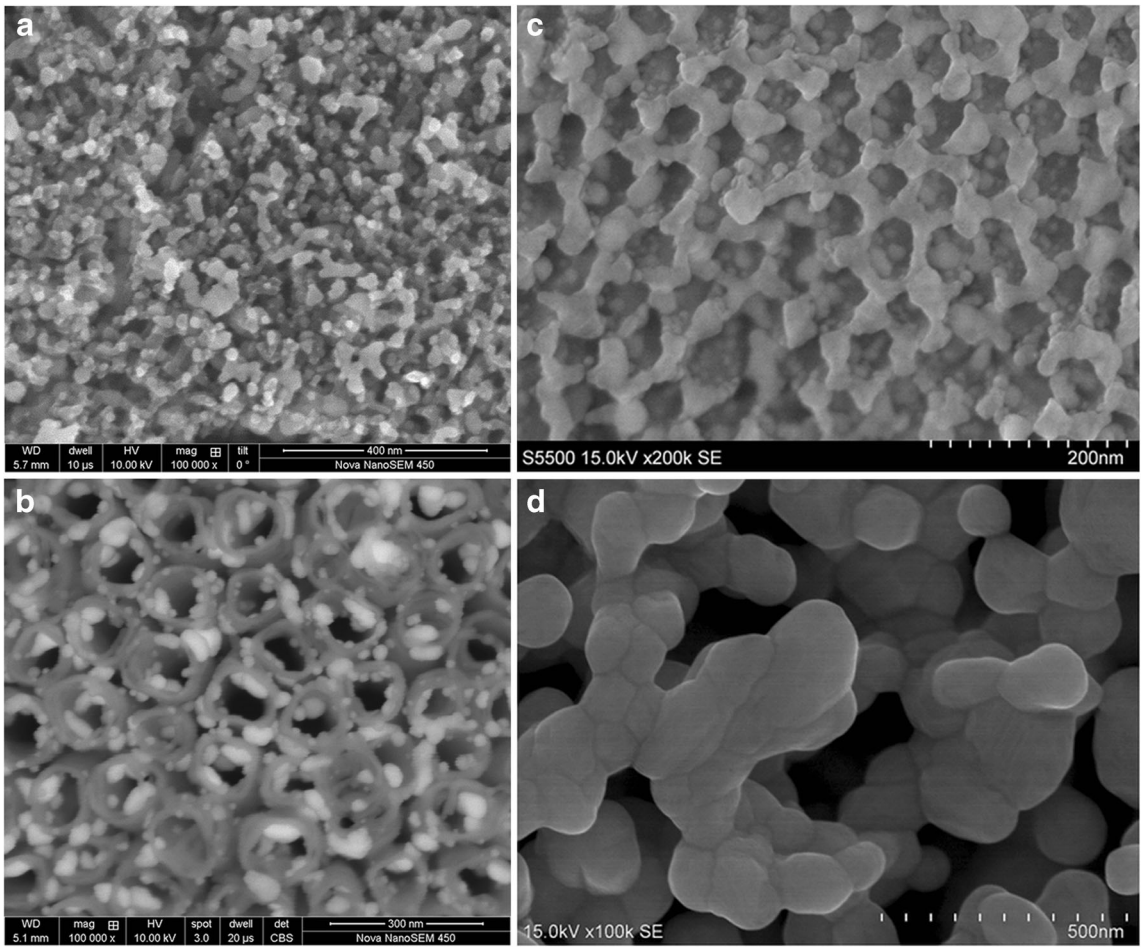

Fig. 4 Top view of TiO_2 nanotubes (10 V, 25 V) and alumina nanoporous structure (15 V) after deposition of silver nanoparticles (0.02 mg/cm^2) (**a**–**c**). Morphology of the silver reference sample, Ag ref. is also presented (**d**). **b** is a BSE image while **a**, **c**–**d** are SE images

composites (see, Fig. 6). SERS intensity of anatase covered with 0.015 mg Ag/cm^2 gives lower signals than rutile covered with only 0.010 mg Ag/cm^2. It may seem, therefore, that the state of the titanium oxide surface—anatase or rutile—is probably in this case insignificant. Therefore, for further experiments, samples with rutile structure (annealed at 650 °C, see Fig. 3) were chosen.

Figure 7a shows typical spectra of pyridine adsorbed on TiO_2 nanotubes (10 V) with silver deposited (0.02 mg/cm^2). Detailed descriptions of the pyridine bands visible in the spectra in Fig. 7a are: 620 cm^{-1}—ν_{6a}, 1,011 cm^{-1}—ν_1, 1,038 cm^{-1}—ν_{12}, 1,215 cm^{-1}—ν_{9a} and 1,595 cm^{-1}—ν_{8a} [39, 40]. All these bands originate from aromatic ring vibrations and exhibit A1 symmetry (for details see reference [39]). We found also that the intensities of the SERS signals of pyridine adsorbed on such substrates are influenced by the nanopore/nanotube size. Apparently, the observed effect of the nanotubes diameter on the SERS intensity is a consequence of the distribution of Ag on the oxide surfaces, see e.g. Fig. 4. On the other hand, the spectra are qualitatively similar to each other. The position of individual SERS signals (the characteristic doublet at 1,011 and 1,038 cm^{-1}) and their intensity ratio do not change significantly with a change in the diameter of the nanotubes. Generally, the spectra of the probe molecule (pyridine) on the substrates containing the same amount of Ag are on average much more intense (e.g. about six times for the 5 V sample) than the reference spectrum measured on a typical SERS-active silver substrate (Ag ref.). The only exception is the 25 V sample; the spectra are less intense (~2 times) than those from a typical Ag reference SERS-active substrate.

Similar correlations were obtained for the other probe molecule—mercaptobenzoic acid (see Fig. 7b). The intensity of the recorded SERS spectra for adsorbed MBA also depends on the diameter of the titania nanotubes (as a consequence on V_{max}). As in the case of pyridine, we do not observe any significant shifts in the position of the characteristic signals for MBA, in particular for the bands which can be assigned to the ν_{12}—1,080 cm^{-1} and ν_{8a}—1,593 cm^{-1} vibrations of the aromatic ring [41–44]. The other characteristic band well

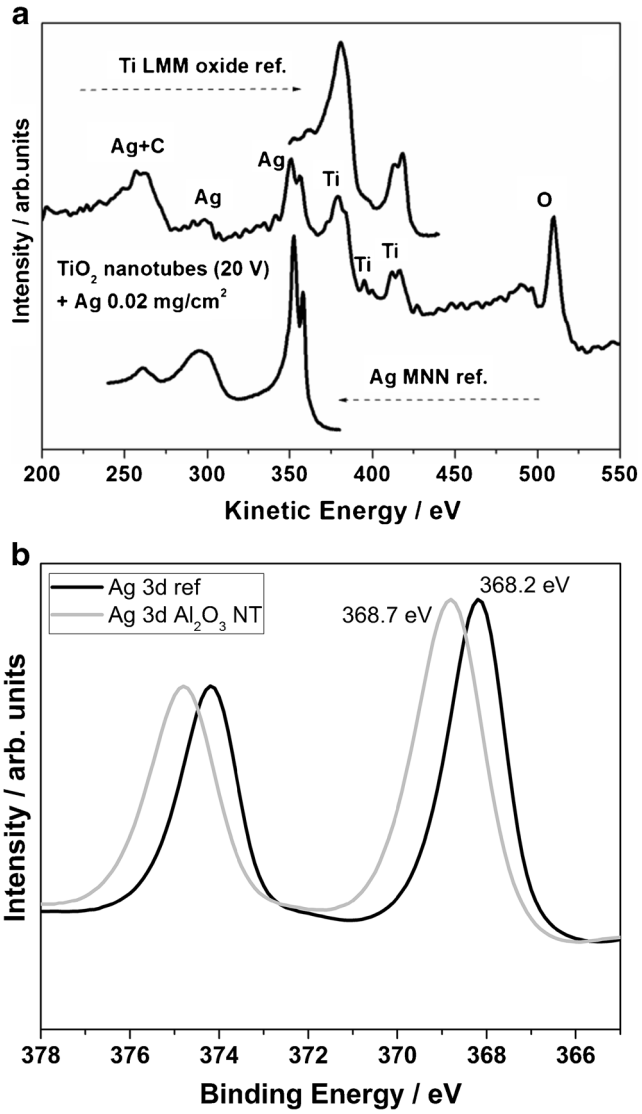

Fig. 5 AES spectrum of Ag/TiO_2—20 V nanotube/Ti sample with 0.02 mg Ag/cm^2. The AES reference spectra for pure Ag and Ti oxide are also given (**a**). XPS spectrum of silver (Ag 3d) recorded on the surface of Ag/Al_2O_3—15 V nanotube/Al with 0.02 mg Ag/cm^2 in relation to Ag ref. (**b**)

visible in the SERS spectrum of MBA is at 1,185 cm^{-1} and is due to the δ(C–H) vibrations [45, 46]. On the basis of the measured SERS spectra it can be easily determine whether the carboxyl group of adsorbed MBA molecules undergoes dissociation during adsorption or not. In the SERS spectra of MBA molecules with non-dissociated carboxyl groups one can see a band at 805 cm^{-1}, whereas for those with dissociated carboxyl groups this spectral region is dominated by a band at 857 cm^{-1} [44, 47, 48]. In the SERS spectrum of MBA adsorbed on the Ag/TiO_2 NT/Ti (Fig. 7b) strong band at 805 cm^{-1} can be seen, while the band at 857 cm^{-1} is absent. This suggests that on Ag/TiO_2 NT/Ti substrate, the carboxyl groups of adsorbed MBA are not dissociated.

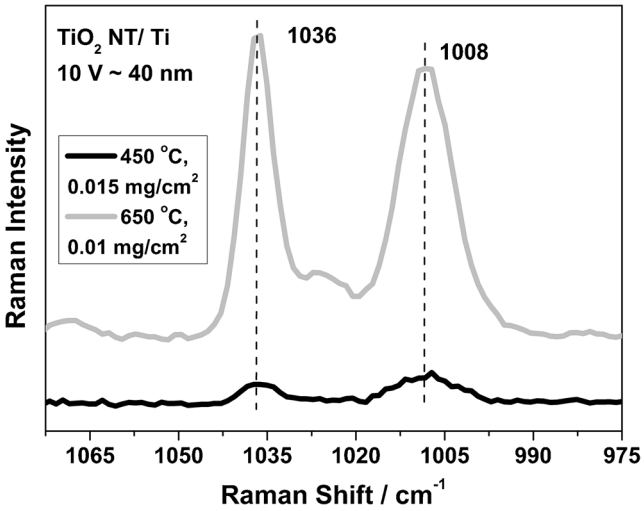

Fig. 6 Effect of thermal treatment of the nanotubular titania—and the resulting change in the titania crystal structure—on the SERS activity of the Ag/TiO_2–NT/Ti samples. Probe molecule—pyridine

The average SERS enhancement factors (E_F) for the Ag/TiO_2–NT/Ti samples are higher than the E_F for the standard Ag ref. substrate measured under the same experimental conditions (see Fig. 8). Thus, our samples may allow to perform effective SERS investigations with the adsorbates, which on a standard rough silver yield only low-intensity signals. The SERS enhancement factors (E_F) for both the pyridine and mercaptobenzoic acid probe molecules were calculated using the following formula (1):

$$E_F = \frac{I_{SERS}}{I_{ref}} \cdot \frac{hc_{ref}}{N_{surf}} \quad (1)$$

where I_{SERS} and I_{ref} are the Raman intensities obtained from the SERS and normal Raman (NR) investigations respectively, c_{ref} stands for the concentration of pure pyridine or pure MBA in the NR measurements and h is the depth-of-focus of the laser beam. The average number of adsorbed molecules per geometric surface area unit participating in the SERS measurements (N_{surf}) was calculated assuming that the adsorbed molecules are spheres closely packed on a plane (a monolayer) to form a hexagonal lattice (densest packing) [19, 49]; formula (2):

$$N_{surf} = A_F \frac{\sqrt{3}}{6} \left(\frac{4\pi}{3}\right)^{2/3} \left(\frac{N_A \rho}{M}\right)^{2/3} \quad (2)$$

where A_F is the surface geometric factor obtained from the AFM measurements, N_A is the Avogadro constant and M and ρ the molar mass and molar density of the pure pyridine or pure mercaptobenzoic acid, respectively.

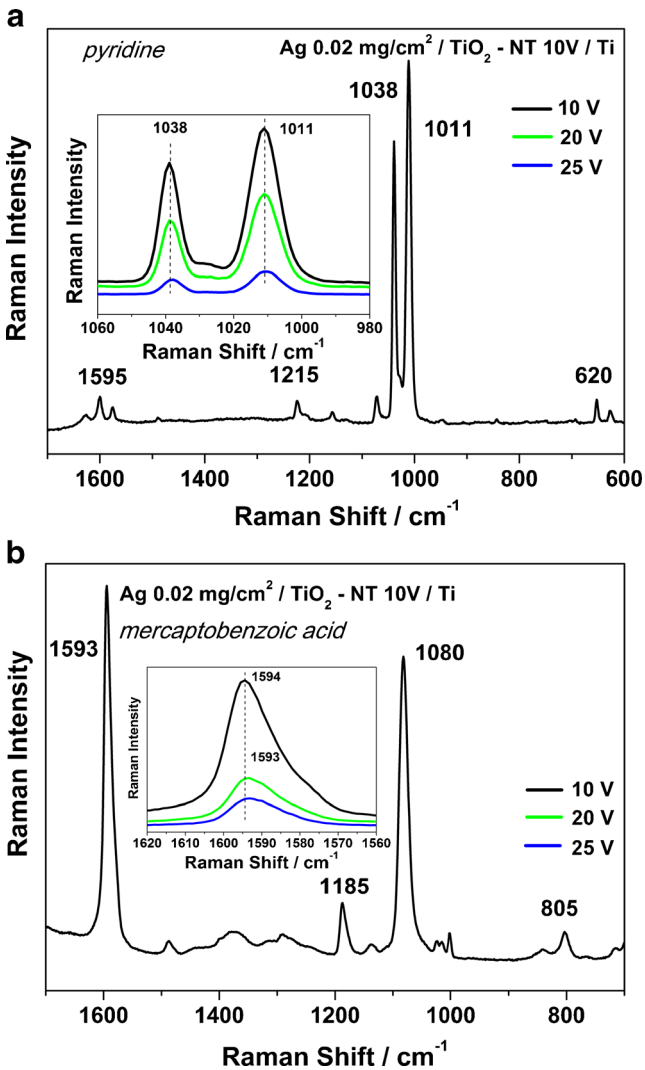

Fig. 7 Typical SERS spectra of 0.05 M pyridine (**a**) and 0.41 M mercaptobenzoic acid (**b**) adsorbed on the surface of the Ag/TiO_2–NT/Ti sample. The *inserts* show SERS spectra for titania nanotubes formed at different V_{max}, and, hence, having different pore diameters

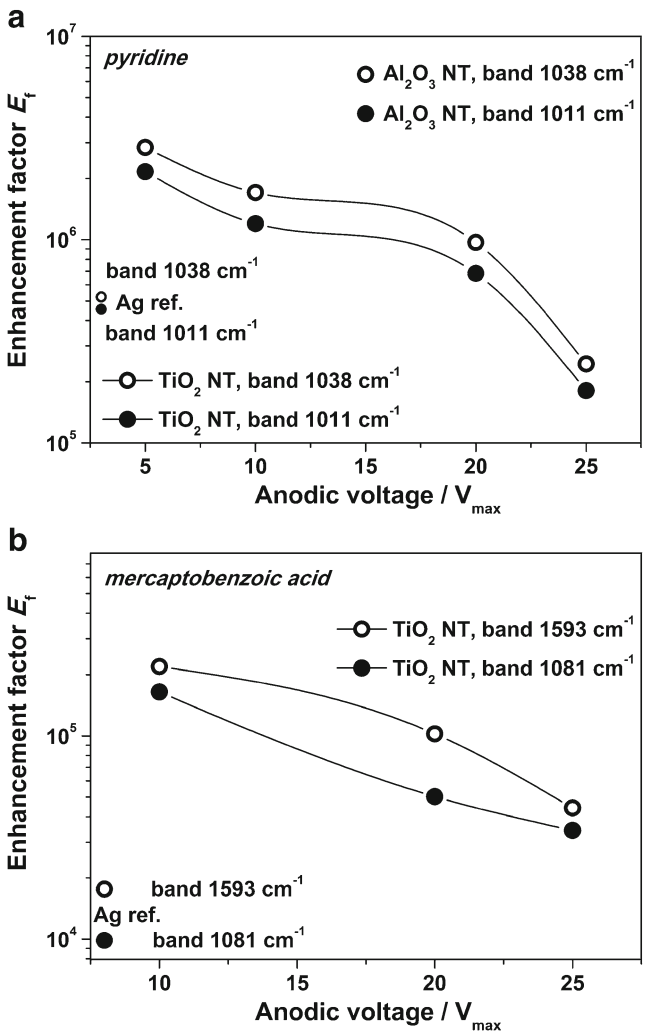

Fig. 8 The dependence between the final voltage V_{max} of formation of the titania nanoporous layers (and hence, the nanotube diameter) in the composite and the resulting SERS enhancement factor E_F calculated from formula (1). Reference data are also shown for Ag ref., and the composite sample based on nanoporous alumina (15 V). Adsorbates: **a** pyridine, **b** mercaptobenzoic acid

Some of the results obtained for the titania nanotubes were compared with the data for alumina produced at V_{max}=15 V (0.02 mg Ag/cm^2). We found that this kind of modified surface gives an even higher enhancement factor than the titania-based surface (see Fig. 8a, b). Moreover, the reproducibility of the SERS signals' intensities was better for the nanoporous alumina than for the standard roughened Ag and titania nanotubes, which is an important factor for potential users of such materials.

For both probe-molecules used for the SERS measurements, similar correlations were observed: the enhancement factors were the highest for the smallest diameters of the nanopores. Such an effect is probably a result of differences in the morphology of the SERS substrates, as shown in Fig. 4a–c. Apparently, the more developed surface area of Ag offers a larger population of active SERS sites (so-called "hot-spots"), such as slits or narrow cavities, which are not detectable by SEM examinations, but which are evidently sensed by the probe molecules. We may thus suspect that the higher E_F is a result of the way the Ag deposit distributes itself on the various nanotubular/nanoporous substrates.

Our suspicion concerning the effect of subtle changes in the morphology of Ag deposit (not detectable using SEM) with time on the E_F have been confirmed by the SERS measurements of the Ag/MeO_x–NT/Me samples after their ageing for 6 months in the laboratory conditions. Ageing in air at room temperature quenches the SERS signals, see SERS spectra shown in the Fig. 9a, b. The degree of the E_F decay (~5 times for TiO_2 NT, ~4 times for Al_2O_3 NT) after 6 months of ageing is shown schematically in Fig. 10. This effect should be taken into account during future analytical applications of the nanoporous layers containing silver as SERS active

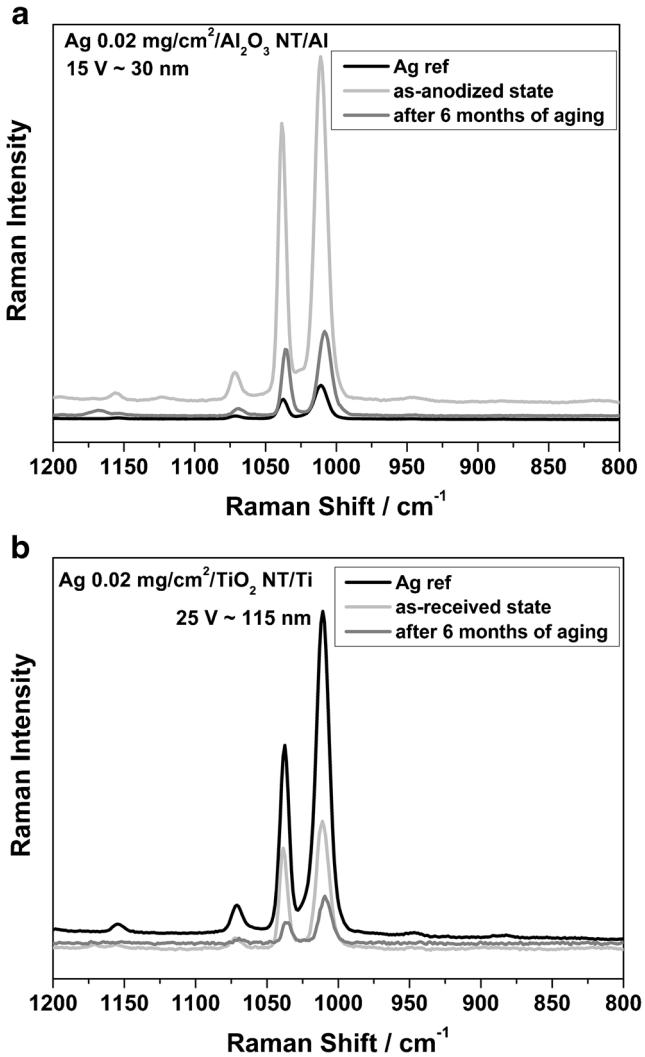

Fig. 9 Effect of ageing of the Ag/MeO_x–NT/Me (**a** Al_2O_3 NT, **b** TiO_2 NT) samples at room temperature on the SERS spectra for pyridine

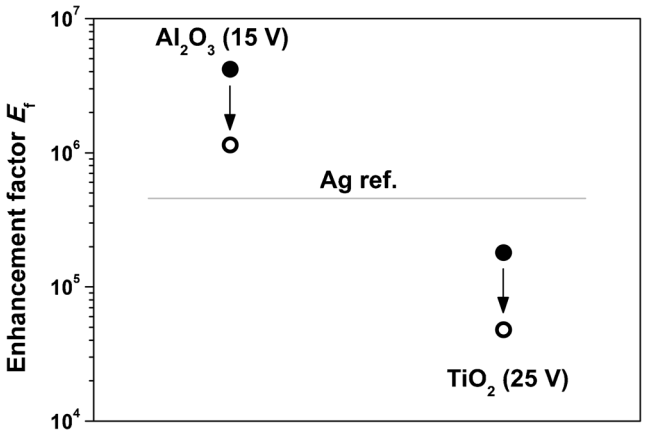

Fig. 10 Schematic representation of the effect of ageing in air of the Ag/MeO_x–NT/Me samples on SERS enhancement factor E_F for adsorbed pyridine: *black circle*—fresh samples, *empty circle*—after 6 months of ageing

substrates. The decrease of SERS signal may result from a restructurization of the unstable Ag deposit distributed on the nanotubular/nanoporous substrate, which, however, is not detectable in SEM examinations, but is evidently sensed by the adsorbed molecules. This may suggest that this restructurization occurs at the scale of a single molecule.

In summary, our investigations have shown that, in Ag/MeO_x–NT/Me samples, TiO_2-based nanoporous substrates are less SERS-efficient than Al_2O_3-based substrates. The enhancement of SERS intensity is not only determined by the morphology and crystal structure of the substrate oxide, but also by chemical effects involving a modification of the electronic properties of the Ag nanoparticles (an interaction between the Ag metal and the nanotubular oxide). This type of interaction was observed not only in the SERS spectra (shifts of the characteristic bands), but also on the AES and XPS spectra of Ag (a shift of peak position, see e.g. Fig. 5b). A detailed discussion can be found elsewhere [19]. Apparently, this phenomenon affects the enhancement factor for pyridine and mercaptobenzoic acid adsorbed on an Ag/Al_2O_3–NT/Al substrate, and accounts for its better reproducibility and stability. The latter two effects were not detected for the titanium-based substrate.

Conclusion

- Nanotubular/porous substrates covered with Ag deposit (Ag/MeO_x–NT/Me) are promising as effective SERS-active platforms. The E_F is the highest for the smallest nanotube diameter. For Ag/Al_2O_3 NT/Al material the E_F of the probe molecules investigated is distinctly higher than that for Ti-based composite, and an order of magnitude higher than that for commonly used in SERS measurements roughened silver, Ag ref.
- Our results show that, in particular, porous alumina interacting with Ag nano-deposits, and hence affecting the electronic structure of the Ag-nanoparticles, may be most useful in detecting small amounts of certain organic compounds and their interaction with composite substrates such as Ag/MeO_x–NT/Me.
- The probe molecules sense even slight changes on the surface, such as distribution of the Ag deposit on the nanotubular structures, which manifest themselves in the SERS intensity. Prolonged ageing in air of the Ag/MeO_x–NT composite layers quenches the SERS signals.

Acknowledgements We are most grateful to Prof. Robert Nowakowski of the Institute of Physical Chemistry PAS (Poland) and Dr Mariusz Andrzejczuk of the Faculty of Materials Science and Engineering, Warsaw University of Technology (Poland) for their cooperation and helpful discussions. This work was financially supported by the National Science Centre (Decision No. DEC-2011/01/

B/ST5/06257) and by the Institute of Physical Chemistry PAS (Warsaw, Poland).

References

1. Liang H-C, Li X-Z, Nowotny J (2010) Photocatalytical properties of TiO_2 nanotubes. Solid State Phenom 162:295–328
2. Zhang Y, Li X, Chen D, Ma N, Hua X, Wang H (2009) Si doping effects on the photocatalytic activity of TiO_2 nanotubes film prepared by an anodization process. Scr Mater 60:543–546
3. Macak JM, Tsuchiya H, Ghicov A, Yasuda K, Hahn R, Bauer S, Schmuki P (2007) TiO_2 nanotubes: self-organized electrochemical formation, properties and applications. Curr Opin Solid State Mater Sci 11:3–18
4. Raja KS, Mahajan VK, Misra M (2006) Determination of photo conversion efficiency of nanotubular titanium oxide photoelectrochemical cell for solar hydrogen generation. J Power Sources 159:1258–1265
5. Macak JM, Barczuk PJ, Tsuchiya H, Nowakowska MZ, Ghicov A, Chojak M, Bauer S, Virtanen S, Kulesza PJ, Schmuki P (2005) Self-organized nanotubular TiO_2 matrix as support for dispersed Pt/Ru nanoparticles: enhancement of the electrocatalytic oxidation of methanol. Electrochem Commun 7:1417–1422
6. Chen B, Hou J, Lu K (2013) Formation mechanism of TiO_2 nanotubes and their applications in photoelectrochemical water splitting and supercapacitors. Langmuir 29:5911–5919
7. Menon L (2009) Porous alumina templates for nanofabrication. Dekker Encycl Nanosci Nanotechnol, Second Edi. Taylor & Francis Group, LLC, pp 3525–3538
8. Sulka GD, Zaraska L, Stepniowski WJ (2009) Anodic porous alumina as a template for nanofabrication. In: Nalwa HS (ed) Encycl Nanosci Nanotechnol. pp 1–89
9. Md Jani AM, Losic D, Voelcker NH (2013) Nanoporous anodic aluminium oxide: advances in surface engineering and emerging applications. Prog Mater Sci 58:636–704
10. Santos A, Kumeria T, Losic D (2013) Nanoporous anodic aluminum oxide for chemical sensing and biosensors. Trends Anal Chem 44: 25–38
11. Brammer KS, Oh S, Frandsen CJ, Jin S (2011) Biomaterials and biotechnology schemes utilizing TiO_2 nanotube arrays. In: Pignatello R (ed) Biomater Sci Eng. InTech, pp 193–210
12. Pittrof A, Bauer S, Schmuki P (2011) Micropatterned TiO_2 nanotube surfaces for site-selective nucleation of hydroxyapatite from simulated body fluid. Acta Biomater 7:424–431
13. Roguska A, Pisarek M, Andrzejczuk M, Dolata M, Lewandowska M, Janik-Czachor M (2011) Characterization of a calcium phosphate-TiO_2 nanotube composite layer for biomedical applications. Mater Sci Eng C 31:906–914
14. Tsuchiya H, Berger S, Macak JM, Munoz A, Schmuki P (2007) A new route for the formation of self-organized anodic porous alumina in neutral electrolytes. Electrochem Commun 9:545–550
15. Wang J, Lin Z (2009) Anodic formation of ordered TiO_2 nanotube arrays: effects of electrolyte temperature and anodization potential. J Phys Chem C 113:4026–4030
16. Shin Y, Lee S (2008) Self-organized regular arrays of anodic TiO_2 nanotubes. Nano Lett 8:3171–3173
17. Roguska A, Kudelski A, Pisarek M, Opara M, Janik-Czachor M (2011) Raman investigations of SERS activity of Ag nanoclusters on a TiO_2-nanotubes/Ti substrate. Vib Spectrosc 55:38–43
18. Pisarek M, Roguska A, Kudelski A, Andrzejczuk M, Janik-Czachor M, Kurzydłowski KJ (2013) The role of Ag particles deposited on TiO_2 or Al_2O_3 self-organized nanoporous layers in their behavior as SERS-active and biomedical substrates. Mat Chem Phys 139:55–65
19. Kudelski A, Pisarek M, Roguska A, Holdynski M, Janik-Czachor M (2012) Surface-enhanced Raman scattering investigations on silver nanoparticles deposited on alumina and titania nanotubes: influence of the substrate material on surface-enhanced Raman scattering activity of Ag nanoparticles. J Raman Spectrosc 43:1360–1366
20. Roguska A, Kudelski A, Pisarek M, Opara M, Janik-Czachor M (2011) Surface-enhanced Raman scattering (SERS) activity of Ag, Au and Cu nanoclusters on TiO_2-nanotubes/Ti substrate. Appl Surf Sci 257:8182–8189
21. Mondal B, Saha SK (2010) Fabrication of SERS substrate using nanoporous anodic alumina template decorated by silver nanoparticles. Chem Phys Lett 497:89–93
22. Nuntawong N, Horprathum M, Eiamchai P, Wong-ek K, Patthanasettakul V, Chindaudom P (2010) Surface-enhanced Raman scattering substrate of silver nanoparticles depositing on AAO template fabricated by magnetron sputtering. Vacuum 84: 1415–1418
23. Huang Y, Sun L, Xie K, Lai Y, Liu B, Ren B, Lin C (2011) SERS study of Ag nanoparticles electrodeposited on patterned TiO_2 nanotube films. J Raman Spectrosc 42:986–991
24. Sharma B, Frontiera RR, Henry A-I, Ringe E, Van Duyne RP (2012) SERS: materials, applications, and the future. Mater Today 15:16–25
25. Cialla D, Marz A, Bohme R, Theil F, Weber K, Schmitt M, Popp J (2012) Surface-enhanced Raman spectroscopy (SERS): progress and trends. Anal Bioanal Chem 403:27–54
26. Kudelski A (2008) Analytical applications of Raman spectroscopy. Talanta 76:1–8
27. Kudelski A (2009) Raman spectroscopy of surfaces. Surf Sci 603: 1328–1334
28. Camargo PHC, Au L, Rycenga M, Li W, Xia Y (2010) Measuring the SERS enhancement factors of dimers with different structures constructed from silver nanocubes. Chem Phys Lett 484:304–308
29. Paczesny J, Kaminska A, Adamkiewicz W, Winkler K, Sozanski K, Wadowska M, Dziecielewski I, Holyst R (2012) Three steps of hierarchical self assembly toward a stable and efficient surface enhanced Raman spectroscopy platform. Chem Mater 24:3667–3673
30. Roguska A, Kudelski A, Pisarek M, Lewandowska M, Kurzydłowski KJ, Janik-Czachor M (2009) In situ spectroelectrochemical surface-enhanced Raman scattering (SERS) investigations on composite Ag/TiO_2-nanotubes/Ti substrates. Surf Sci 603:2820–2824
31. Sulka GD, Stępniowski WJ (2009) Structural features of self-organized nanopore arrays formed by anodization of aluminum in oxalic acid at relatively high temperatures. Electrochim Acta 54: 3683–3691
32. Yang B, Ng CK, Fung MK, Ling CC, Djurišić AB, Fung S (2011) Annealing study of titanium oxide nanotube arrays. Mater Chem Phys 130:1227–1231
33. Yu J, Wang B (2010) Effect of calcination temperature on morphology and photoelectrochemical properties of anodized titanium dioxide nanotube arrays. Appl Catal B Environ 94:295–302
34. Jaroenworaluck A, Regonini D, Bowen CR, Stevens R (2010) A microscopy study of the effect of heat treatment on the structure and properties of anodised TiO_2 nanotubes. Appl Surf Sci 256:2672–2679
35. Kneipp K, Moskovits M, Kneipp H (2006) Surface-enhanced Raman scattering. Springer, Germany
36. Stiles PL, Dieringer JA, Shah NC, Van Duyne RP (2008) Surface-enhanced Raman spectroscopy. Annu Rev Anal Chem 1:601–626

37. Du Y, Shi L, He T, Sun X, Mo Y (2008) SERS enhancement dependence on the diameter and aspect ratio of silver-nanowire array fabricated by anodic aluminium oxide template. Appl Surf Sci 255: 1901–1905
38. Chastain J, King RC Jr (1995) Handbook of X-ray photoelectron spectroscopy. Physical Electronics, INC., Eden Praire
39. Urena FP, Gomez MF, Gonzalez JJL, Torres EM (2003) A new insight into the vibrational analysis of pyridine. Spectrochim Acta A 59:2815–2839
40. Pettinger B, Wetzel H (1981) Surface enhanced Raman scattering from pyridine, water, and halide ions on Au, Ag and Cu electrodes. Ber Bunsenges Phys Chem 85:473–481
41. Michota A, Bukowska J (2003) Surface-enhanced Raman scattering (SERS) of 4-mercaptobenzoic acid on silver and gold substrates. J Raman Spectrosc 34:21–25
42. Yuan Y-X, Ling L, Wang X-Y, Wang M, Gu R-A, Yao J-L (2007) Surface enhanced Raman spectroscopic readout on heavy metal ions based on surface self assembly. J Raman Spectrosc 38:1280–1287
43. Olson TY, Schwartzberg AM, Orme CA, Talley CE, O'Connell B, Zhang JZ (2008) Hollow gold-silver double-shell nanospheres: structure, optical absorption, and surface-enhanced Raman scattering. J Phys Chem C 112:6319–6329
44. Bishnoi SW, Rozell CJ, Levin CS, Gheith MK, Johnson BR, Johnson DH, Halas NJ (2006) All-optical nanoscale pH meter. Nano Lett 6: 1687–1692
45. Orendorff CJ, Gole A, Sau TK, Murphy CJ (2005) Surface-enhanced Raman spectroscopy of self-assembled monolayers: sandwich architecture and nanoparticle shape dependence. Anal Chem 77:3261–3266
46. Lee SB, Kim K, Kim MS (1991) Surface-enhanced Raman scattering of *o*-mercaptobenzoic acid in silver sol. J Raman Spectrosc 22:811–817
47. Kneipp J, Kneipp H, Wittig B, Kneipp K (2007) One- and two-photon excited optical pH probing for cells using surface-enhanced Raman and hyper-Raman nanosensors. Nano Lett 7:2819–2823
48. Talley CE, Jusinski L, Hollars CW, Lane SM, Huser T (2004) Intracellular pH sensors based on surface-enhanced Raman scattering. Anal Chem 76:7064–7068
49. Toth LF (1943) Uber die dichteste kuegllagerung. Math Z 48:676–684